



Contents lists available at ScienceDirect

European Journal of Medicinal Chemistry

journal homepage: www.elsevier.com/locate/ejmech

Research paper

8-Amide and 8-carbamate substitution patterns as modulators of 7-hydroxy-4-methylcoumarin's antidepressant profile: Synthesis, biological evaluation and docking studies

María J. Matos^{a,b,1,*}, Paula Novo^c, Lucía Mayán^c, Iria Torres^c, Eugenio Uriarte^{b,d}, Matilde Yáñez^e, José Ángel Fontenla^e, Francesco Ortuso^{f,g}, Stefano Alcaro^{f,h}, Francesca Procopio^f, María Isabel Rodríguez-Francoⁱ, Cristina Val^{c,e}, María I. Loza^{c,e}, José Brea^{c,e}, Fernanda Borges^a, Dolores Viña^{c,e,**,1}

^a Centro de Investigação em Química da Universidade do Porto (CIQUP), Departamento de Química e Bioquímica, Faculdade de Ciências, Universidade do Porto, rua do Campo Alegre s/n, 4169-007, Porto, Portugal

^b Departamento de Química Orgánica, Facultad de Farmacia, Universidade de Santiago de Compostela, 15782, Santiago de Compostela, Spain

^c Center for Research in Molecular Medicine and Chronic Diseases, University of Santiago de Compostela, 15782, Santiago de Compostela, Spain

^d Instituto de Ciencias Químicas Aplicadas, Universidad Autónoma de Chile, 7500912, Santiago, Chile

^e Departamento de Farmacología, Farmacia y Tecnología Farmacéutica, Universidade de Santiago de Compostela, 15782, Santiago de Compostela, Spain

^f Department of Health Sciences, University "Magna Graecia" of Catanzaro, Campus Universitario "S. Venuta", Viale Europa, Loc. Germaneto, 88100, Catanzaro, Italy

^g Net4Science srl., c/o University "Magna Graecia" of Catanzaro, Campus Universitario "S. Venuta", Viale Europa, Loc. Germaneto, 88100, Catanzaro, Italy

^h CRISEA - Centro di Ricerca e Servizi Avanzati per l'Innovazione Rurale, 88055, Belcastro, Italy

ⁱ Instituto de Química Médica, Consejo Superior de Investigaciones Científicas (IQM-CSIC), C/ Juan de la Cierva, 3, 28006, Madrid, Spain



ARTICLE INFO

Keywords:

Amidocoumarins
Carbamatecoumarins
Monoamine oxidase A
Depression
Docking

ABSTRACT

Psychiatric and neurological disorders affect millions of people worldwide. Currently available treatments may help to improve symptoms, but they cannot cure the diseases. Therefore, there is an urgent need for potent and safe therapeutic solutions. 8-Amide and 8-carbamatecoumarins were synthesized and evaluated as human monoamine oxidase A and B (hMAO-A and hMAO-B) inhibitors. Comparison between both scaffolds has been established, and we hypothesized that the introduction of different substituents can modulate hMAO activity and selectivity. *N*-(7-Hydroxy-4-methylcoumarin-8-yl)-4-methylbenzamide (**9**) and ethyl *N*-(7-hydroxy-4-methylcoumarin-8-yl)carbamate (**20**) proved to be the most active and selective hMAO-A inhibitors (IC₅₀ = 15.0 nM and IC₅₀ = 22.0 nM, respectively), being compound **9** an irreversible hMAO-A inhibitor twenty-four times more active *in vitro* than moclobemide, a drug used in the treatment of depression and anxiety. Based on PAMPA assay results, both compounds proved to be good candidates to cross the blood-brain barrier. In addition, these compounds showed non-significant cytotoxicity on neuronal viability assays. Also, the best compound proved to have a *t*_{1/2} of 6.84 min, an intrinsic clearance of 195.63 μL min⁻¹ mg⁻¹ protein, and to be chemically stable at pH 3.0, 7.4 and 10.0. Docking studies were performed to better understand the binding affinities and selectivity profiles for both hMAO isoforms. Finally, theoretical drug-like properties calculations corroborate the potential of both scaffolds on the search for new therapeutic solutions for psychiatric disorders as depression.

* Corresponding author. Departamento de Química Orgánica, Facultad de Farmacia, Universidade de Santiago de Compostela, 15782, Santiago de Compostela, Spain.

** Corresponding author. Center for Research in Molecular Medicine and Chronic Diseases, University of Santiago de Compostela, 15782, Santiago de Compostela, Spain.

E-mail addresses: mariajoao.correiapinto@usc.es (M.J. Matos), mdolores.vina@usc.es (D. Viña).

¹ These authors contributed equally.

<https://doi.org/10.1016/j.ejmech.2023.115091>

Received 30 September 2022; Received in revised form 27 December 2022; Accepted 3 January 2023

Available online 7 January 2023

0223-5234/© 2023 The Authors. Published by Elsevier Masson SAS. This is an open access article under the CC BY-NC-ND license (<http://creativecommons.org/licenses/by-nc-nd/4.0/>).

1. Introduction

Human monoamine oxidases A and B (*h*MAO-A and *h*MAO-B) are well known targets for psychiatric and neurological disorders [1]. Both isoforms are responsible for the deamination of specific endogenous and exogenous amines [2]. Comparing the amino acid sequences of both human liver MAO-A and MAO-B, it has been proved that they have a similarity of approximately 70% [3]. Despite several MAO-A inhibitors have been described in scientific bibliographic sources, only moclobemide is currently in clinical use to treat certain types of mental depression [4]. Isocarboxazid, phenelzine and tranylcypromine, three irreversible and non-selective MAO inhibitors, are also used as antidepressants, as well as selegiline, a MAO-B selective inhibitor with synergistic antidepressant-like activity. Pargyline and clorgyline are both MAO-A inhibitors with antidepressant profile, but not in clinical use at the moment. Therefore, the search for novel selective *h*MAO-A inhibitors is still an emergent and attractive topic in medicinal chemistry [5].

Over more than ten years, our research group has been looking for potent and selective *h*MAO inhibitors containing the coumarin scaffold (Fig. 1) [6,7]. Most of the studied 3-arylcoumarins proved to selectively inhibit the *h*MAO-B isoform, in most of the cases in the low nanomolar range [8–10]. Different substituents as i.e. methyl, methoxy, hydroxy, nitro and ethoxy, and different atoms, as i.e. halogens, were introduced to establish structure-activity relationships. Also, different positions on both aromatic rings have been explored (Fig. 1A) [11,12].

Using a rational design of new molecules, expanding the chemical space, a carbonyl group was included as a bridge between the coumarin and the extra aromatic ring at position 3 (Fig. 1B) [13]. The design of new 3-benzoylcoumarins tended to give rise to selective *h*MAO-A inhibitors in the micromolar range. Increasing the linkers between the coumarin and the aromatic ring at position 3, 3-carboxamidocoumarins were studied (Fig. 1C) [14,15]. Surprisingly, these compounds turned to be potent and selective *h*MAO-B inhibitors. The success in the pursuit of

potent and selective *h*MAO-B inhibitors continued with new series of amides (Fig. 1D) and carbamates [16–18]. Multitarget molecules have been found, and the arsenal of interesting molecules exponentially increased.

To try to modify the pattern of activity and selectivity against *h*MAOs, changes in the position of the substituents in the coumarin scaffold have been planned (Fig. 1E). Moreover, in the last years, coumarin derivatives have rarely been described as potent and selective MAO-A inhibitors. Recently, 7,8-dihydroxy-4-methylcoumarin has been reported for its capacity of alleviating chronic unpredictable mild stress (CUMS)-induced depression-like behaviours in rats [19]. Besides playing an interesting role in protecting the nervous system, this molecule proved to be safe. In addition, osthonol, a 7-hydroxy-8-prenylated coumarin, has been recently described as a high selective MAO-A inhibitor [20]. In the same study, isopsoralen and bakuchicin, two furanocoumarin derivatives, proved to have similar IC₅₀ values against this enzyme. However, they proved to be non-selective molecules. This information motivated us to design a new series of 7-hydroxy-4-methylcoumarins. As position 8 has been less explored over the years, different amides and carbamates have been introduced at this position, maintaining a hydroxyl group at position 7 and a methyl group at position 4 of the coumarin scaffold. In order to find new alternatives in the design of *h*MAO inhibitors, and based on previous studies from our research group, the *h*MAO inhibitory activities of coumarins with an 8-amide or 8-carbamate substitution patterns, have been studied. Interestingly, this structural modification allowed to discover a new class of highly potent and selective *h*MAO-A inhibitors, focusing our research on the field of neurological diseases such as anxiety and depression.

2. Results and discussion

The studied derivatives were efficiently synthesized according to the protocol outlined in Scheme 1. Coumarins 1–25 were prepared by

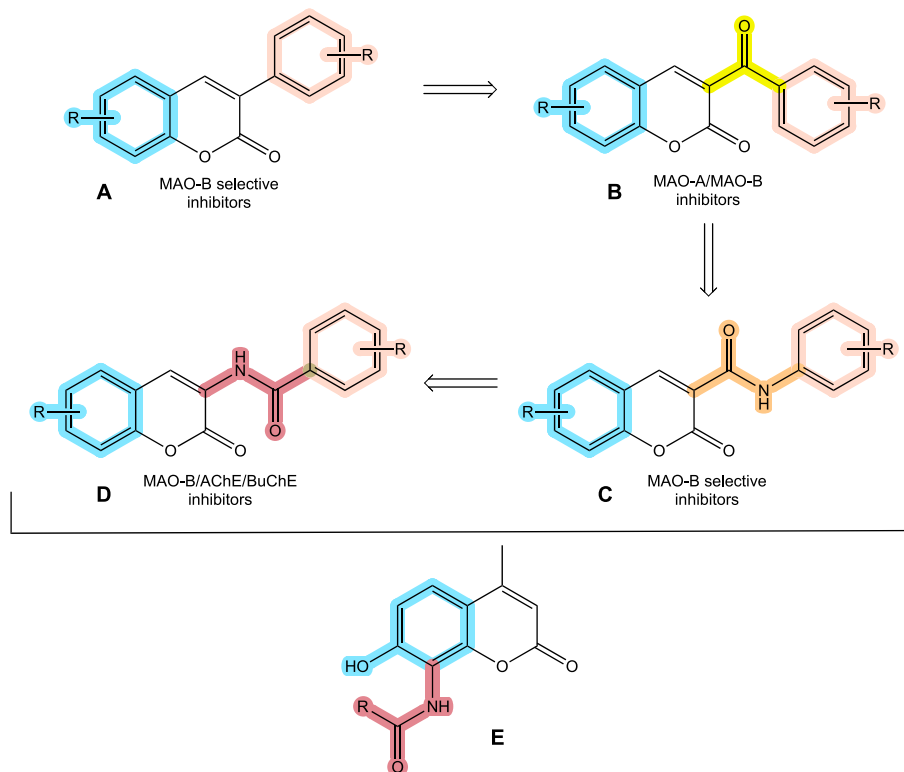
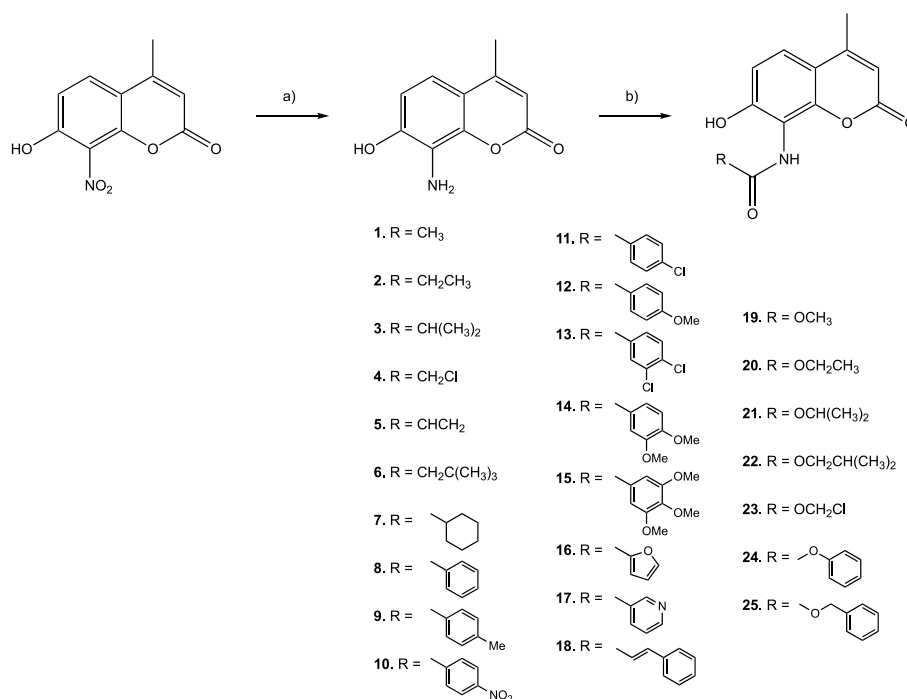


Fig. 1. Rational for the selection of the studied scaffold. A. 3-Arylcoumarin scaffold; B. 3-Benzoylcoumarin scaffold; C. 3-Carboxamidocoumarin scaffold; D. 3-Amidocoumarin scaffold and E. 8-Amidocoumarin and 8-carbamatecoumarin scaffolds, the scope of the current study.



Scheme 1. Synthetic methodology. Reagents and conditions: a) H₂, ethanol, Pd/C, r.t., 5 h; b) Acyl chloride, pyridine, dichloromethane, 0 °C to r.t., overnight.

starting from the 8-amino-7-hydroxy-4-methylcoumarin. This coumarin was obtained by a reduction of the commercially available 7-hydroxy-4-methyl-8-nitrocoumarin, in ethanol, using palladium on carbon (Pd/C) as catalyst, in hydrogen gas (H₂) atmosphere for 5 h, with a yield of 90%. Acylation of the 8-amino-7-hydroxy-4-methylcoumarin with the conveniently substituted acid chloride, using pyridine in dichloromethane, from 0 °C to room temperature (r.t.), afforded a variety of 8-amide and 8-carbamate substituted coumarins 1–25, in yields between 80 and 92%. The reaction conditions and characterization of the new compounds are detailed in the Experimental Section and in the Supporting Information.

Activity of these compounds on recombinant *h*MAO activity was investigated by measuring their effects on the production of H₂O₂ from *p*-tyramine (a common substrate for *h*MAO-A and *h*MAO-B), using the Amplex Red MAO assay kit and microsomal MAO isoforms prepared from insect cells (BTITN-5B1-4) infected with recombinant baculovirus containing cDNA inserts for *h*MAO-A or *h*MAO-B. Most of the tested compounds proved to inhibit the enzymatic activity in a concentration-dependent manner, and the experimental IC₅₀ results are listed in Table 1.

Coumarins have been widely substituted for their potential on the search of new potent and safe compounds against different targets involved on neurological and neuropsychiatric disorders. Position 8 of this scaffold has been less explored on MAO inhibition studies. Therefore, and based on the interest of 3-amidocoumarins and 3-carbamate-coumarins previously studied by the group [17–19], we designed and synthesized a family of twenty-five compounds presenting structural diversity: lineal, cyclic, electron withdrawing and electron donating groups have been attached to the amide or carbamate function at position 8 in order to establish some preliminary structure-activity relationships.

As shown in Table 1, and aligned with previously reported results for 3-amide and 3-carbamate derivatives, five of the studied compounds (4, 6, 13, 16 and 24) displayed selective inhibitory activity against *h*MAO-B in the micromolar range, being 3,4-dichloro-*N*-(7-hydroxy-4-methylcoumarin-8-yl)benzamide (13) the most active derivative of the series (IC₅₀ = 2.29 μM). Surprisingly, fourteen out of twenty-five compounds in this study showed *h*MAO-A affinity, being five compounds selective

against this isoform (9, 12, 14, 18 and 20) in the low micro and nanomolar ranges.

N-(7-Hydroxy-4-methylcoumarin-8-yl)-4-methylbenzamide (9) and ethyl (7-hydroxy-4-methylcoumarin-8-yl)carbamate (20) proved to be the most potent derivatives (IC₅₀ = 15 nM and IC₅₀ = 22 nM, respectively). Compound 9 is more than 6,666.67-fold selective over *h*MAO-B and, therefore, is the most *h*MAO-A selective compound from the studied series, being also the best *h*MAO-A selective inhibitor reported by the group so far. It is remarkable that this compound is twenty-four times more active than moclobemide, the reference compound, a reversible inhibitor drug used in the treatment of depression and anxiety.

Nine of the studied coumarins (1, 5, 7, 10, 11, 17, 21, 23 and 25) inhibit both MAO isoforms, with IC₅₀ values and selectivity profiles similar to iproniazid. Iproniazid, also used as reference compound, is a non-selective, irreversible MAO inhibitor of the hydrazine family. In general, it can be observed that carbamates are more potent than the corresponding amide derivatives. However, selectivity cannot be clearly established based on this classification. Modulating the size and nature of the side chains of both scaffolds may lead to selective or dual inhibitors.

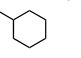
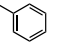
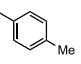
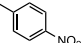
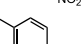
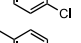
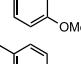
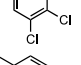
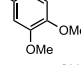
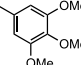
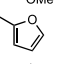
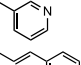
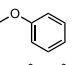
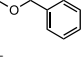
The mode of inhibition produced by the best compound (9) was also characterized by using an effective dilution method (Fig. 2). Clorgyline, an irreversible MAO-A inhibitor (IC₅₀ = 1.0 ± 0.03 nM), was used as control [21].

Fig. 2 shows that compound 9 inhibits the activity of *h*MAO-A in an irreversible mode, similarly to the reference inhibitor, clorgyline. There is still high controversy regarding the mode of inhibition that provides more benefits in clinical practice. Researchers supporting the advantages of irreversible MAO inhibitors argue that they are more potent than reversible ones, proposing that reversible inhibitors may not be effective enough [22,23]. Therefore, this may not be considered a constrain for the high potential of this molecule as *h*MAO-A inhibitor.

In addition to the *h*MAO-A and *h*MAO-B inhibitory activities, it would be interesting that the studied compounds do not display cytotoxic effects, in order to maintain neuronal populations that are affected during the establishment and evolution of neurodegenerative diseases. Therefore, the *in vitro* cytotoxic activity on the SH-SY5Y cell line has been studied, and the results presented in Fig. 3. All the compounds have

Table 1

IC₅₀ values of the studied molecules (new compounds 1–25 and reference inhibitors) on the enzymatic activity of hMAO expressed in baculovirus infected BTI insect cells.

Compounds	R	IC ₅₀ hMAO-A (μM)	IC ₅₀ hMAO-B (μM)	SI ^a
1	CH ₃	27.30 ± 1.82	31.15 ± 2.09	1.14
2	CH ₂ CH ₃	*	*	–
3	CH(CH ₃) ₂	*	*	–
4	CH ₂ Cl	*	52.68 ± 3.53	<0.52 ^b
5	CHCH ₂	38.10 ± 2.55	31.05 ± 2.08	0.81
6	CH ₂ C(CH ₃) ₃	*	85.89 ± 5.76	<0.86 ^b
7		13.33 ± 0.89	16.27 ± 1.09	1.22
8		*	**	–
9		0.015 ± 0.001	**	>6,666.67 ^b
10		4.14 ± 0.45	7.35 ± 0.85	1.78
11		38.70 ± 2.59	50.33 ± 3.34	1.30
12		0.498 ± 0.043	12.56 ± 3.26	25.22
13		20.11 ± 1.35	2.29 ± 0.15	0.11
14		1.09 ± 0.21	*	>91.74 ^b
15		*	**	–
16		**	84.83 ± 5.69	<0.85 ^b
17		31.32 ± 2.10	37.26 ± 2.49	1.19
18		0.336 ± 0.003	6.24 ± 0.59	8.57
19	OCH ₃	*	**	–
20	OCH ₂ CH ₃	0.022 ± 0.003	*	>4,545.45 ^b
21	OCH(CH ₃) ₂	1.88 ± 0.44	2.47 ± 0.16	1.31
22	OCH ₂ CH(CH ₃) ₂	*	*	–
23	OCH ₂ Cl	9.19 ± 2.60	9.11 ± 0.90	0.99
24		*	68.29 ± 4.31	<0.68 ^b
25		17.18 ± 0.75	17.34 ± 0.76	1.01
Iproniazid	–	6.56 ± 0.76	7.54 ± 0.36	1.15
Moclobemide	–	0.36 ± 19.30	**	>277.78 ^b

Each IC₅₀ value is the mean ± s.e.m. of 3 experiments (n = 3).

* Inactive at 100 μM.

** At 100 μM, inhibits ~50% of the activity. At higher concentrations, the compounds precipitate.

^a MAO-A selectivity index (SI) expressed as [IC₅₀ (MAO-B)]/[IC₅₀ (MAO-A)].

^b Value calculated considering the IC₅₀ against MAO-A or MAO-B > 100 μM.

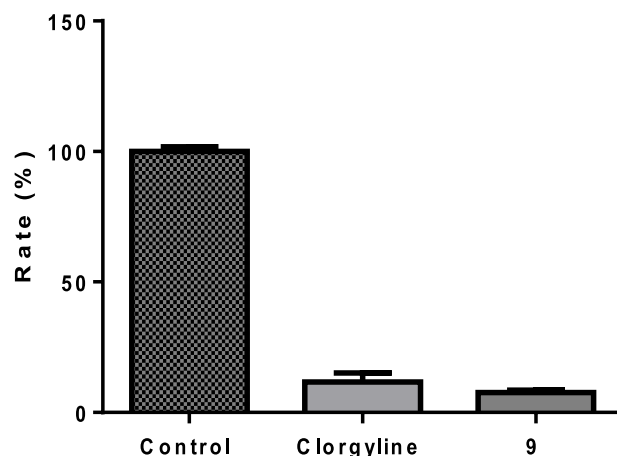


Fig. 2. Recovery of hMAO-A activity treated with clorgyline or compound 9 (after 40 min of preincubation and dilution from 10xIC₅₀ to 0.1xIC₅₀) and enzymatic activity of the control. Data are the mean ± s.e.m.

been studied at 100 μM, the highest concentration used on the MAO assays.

Fortunately, in SH-SY5Y cells toxicity studies, only compound 24 showed statistically significant toxicity at the studied concentration (100 μM) (Fig. 3). This data highlights the potential of the scaffold, and the selected substitution patterns, on the design of new potent, effective and safe molecules.

In vitro metabolic stability of compound 9 using human and mouse liver microsomes has been performed, and the stability parameters obtained are summarized in Table 2. The metabolic stability has been calculated from the logarithm of the remaining compound at each time evaluated. The percentage remaining after incubation for 60 min in the presence of human microsomes has been 0.5%, while in the presence of mouse microsomes, 8.3% of parent compound was still present. The calculated t_{1/2} has been 6.84 min in human and 17.10 min in mouse. The intrinsic clearance (μL min⁻¹ mg⁻¹ protein) determined led to a 195.63 value for human and 131.46 for mouse samples (the chart is included in the Supporting Information).

In order to evaluate chemical stability, overnight incubations of compound 9 (10 μM) at room temperature and different pH (3.0, 7.4 and 10.0), were carried out (Table 3). Aliquots at t = 0 and after incubation have been taken, and analysed by UPLC-MS/MS (all the chromatograms are included in the Supporting Information). As observed, compound 9 proved to be stable in all the conditions tested.

Brain penetration was predicted using the *in vitro* PAMPA-BBB assay described by Di et al. [24], partially modified by a part of us for testing molecules with limited water-solubility [25–28]. The permeability value (P_e) of compounds 9 and 20 through a lipid extract of porcine brain was determined by using PBS:ethanol (70:30) as solvent, during 2 h, at room temperature, and results are gathered in Table 4. In the same assay, 10 commercial drugs of known central nervous systems (CNS) penetration were also tested and their permeability values were compared and normalized to the reported data. According to the patterns previously established in the bibliography, compounds with P_e exceeding 4·10⁻⁶ cm s⁻¹ would be able to cross the blood-brain barrier (BBB), whereas those displaying P_e less than 2·10⁻⁶ cm s⁻¹ would not reach the CNS. Compounds 9 and 20 showed permeability values above 4·10⁻⁶ cm s⁻¹ in this *in vitro* BBB model (Table 4) and thus, it is expected that they may enter into the CNS by passive diffusion and interact with their biological

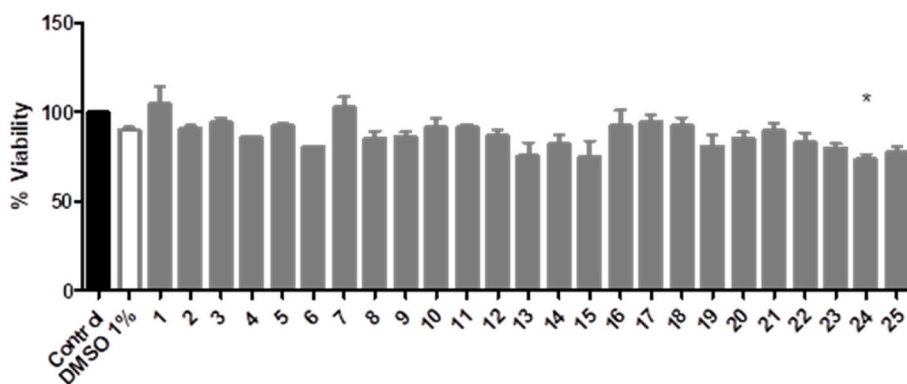


Fig. 3. Effect of the compounds on the viability of the SH-SY5Y cell line after 24 h of incubation. The results are expressed as the average of viability of at least 3 experiments \pm s.e.m. comparing to the vehicle (DMSO 1%) treated group. The results were analysed with an ANOVA statistical test, followed by Bonferroni's multiple comparison test. * Level of statistical significance $P < 0.05$.

Table 2

Microsomal stability parameters obtained for compound 9.

	% remanent (sampling time 60 min)	$t_{1/2}$ (min)	Clint ($\mu\text{L}/\text{min}\cdot\text{mg}$ prot)
Human	0.5	6.84	195.63
Mouse	8.3	17.10	131.46

Table 3

Chemical stability parameters obtained for compound 9.

	% remaining
pH 3.5	98.0
pH 7.4	113.2
pH 10.5	117.6

Table 4

Permeability values from the PAMPA-BBB assay P_e ($10^{-6} \text{ cm s}^{-1}$) of compounds 9 and 20.^a

Compounds	PAMPA-BBB	
	P_e ($10^{-6} \text{ cm s}^{-1}$)	Prediction
9	8.6 ± 0.7	CNS +
20	4.9 ± 0.1	CNS +

^a Results are the mean \pm SD of three independent experiments.

targets.

The targets' recognition of the most potent inhibitors (9 and 20) was investigated by means of molecular modelling. In general, the docking results were not clearly in accordance with the experimental inhibition. In fact, docking did not reveal substantial differences in terms of theoretical binding affinity for 9 and 20 against *h*MAO-A and *h*MAO-B (Table S1). However, analysis of the best binding energy poses shows a different orientation of the two compounds in the catalytic site of targets. In detail, small substituents such as propylcarbamate (20, Fig. 4B) are oriented towards the FAD cofactor in *h*MAO-A, while bulkier moieties, such as *p*-methylphenylamide (9, Fig. 4A), show an opposite orientation, with the substituent facing the entrance of the catalytic pocket. Conversely, in the *h*MAO-B, the substituents at position 8 are always oriented towards the entrance of the catalytic site (Fig. S1). In order to better investigate the ligand-target recognition, 50 ns of molecular dynamics (MD) were performed on each ligand-target docking top ranked complex.

MD simulation on *h*MAO-A complexes, reported the 9 coumarin nucleus and the *p*-methylphenyl substituent engaging stacking with

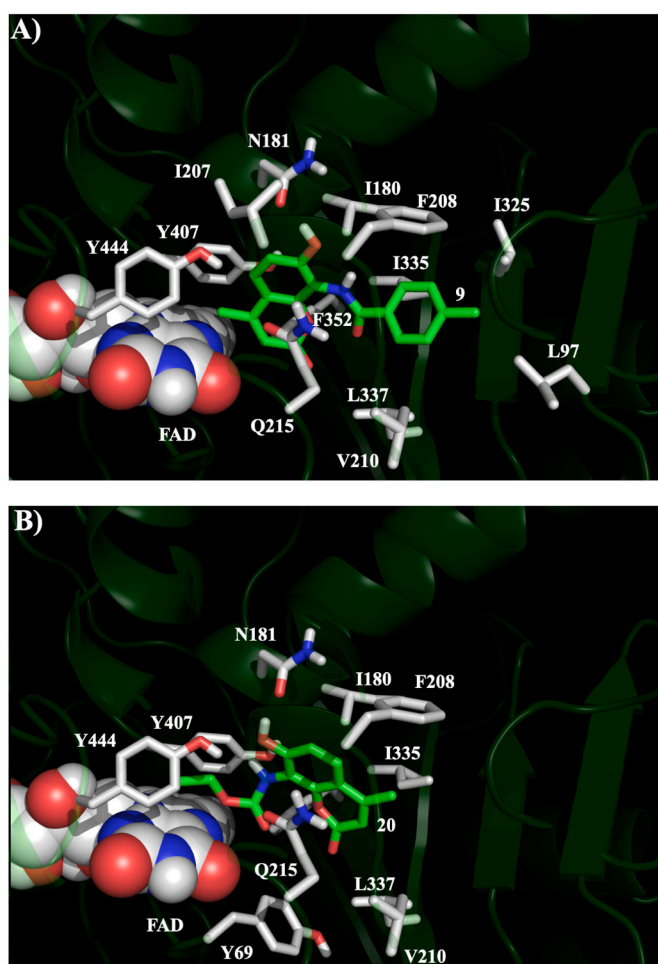


Fig. 4. Best docking poses of compounds 9 (A) and 20 (B) in the active site of *h*MAO-A. Ligands are reported in green carbon-colored sticks, interacting residues are depicted in white carbon-colored sticks and FAD cofactor is shown as CPK sphere.

Phe352, in 11% of the MD sampled structures (MDSS), Tyr407, in 28% MDSS, and Phe208, in 79% MDSS (Fig. S2). The hydroxyl group at position 7, instead, established a stable hydrogen bond with the Asn181 (97% MDSS). Several favorable hydrophobic contacts among 9 and catalytic site residues were also highlighted. In compound 20 simulation (Fig. S3), the ligand hydroxyl group at position 7 was involved in

hydrogen bonds with Asn181 (77% MDSS) and Tyr444 (36%). Several stackings were observed between the inhibitor's coumarin moiety and Tyr69 (25% MDSS), Phe352 (47% MDSS) and Phe208 (25% MDSS). The sp^2 oxygen of the carbamate linker was involved in hydrogen bond with Gln215 (49% MDSS) and Tyr444 (10% MDSS).

The **9** recognition of *h*MAO-B (Fig. S4) was stabilized by stacking between ligand coumarin nucleus and Phe343 (11% MDSS) and Tyr398 (42% MDSS), and between the toluene moiety and Tyr326 (30% MDSS). Hydrogen bonds were observed between the amidic sp^2 oxygen of **9** and Ser200 (36% MDSS), and between the ligand hydroxyl group at position 7 and Ile198 (37% MDSS). In *h*MAO-B, compound **20** reported an intramolecular hydrogen bond between substituents at positions 7 and 8 (76% MDSS) (Fig. S5). Carbamate nitrogen and lactamic sp^2 oxygen were interacting, by hydrogen bonds, with Tyr326 (18% MDSS) and Ser200 (18% MDSS), respectively. Stackings were observed between the ligand coumarin moiety and *h*MAO-B Tyr326 (6% MDSS), Phe343 (3% MDSS) and Tyr398 (26% MDSS).

Considering MD recognition analysis, reporting for both **9** and **20** more durable interactions in *h*MAO-A than in *h*MAO-B complexes, a qualitative accordance between theoretical and experimental data can be observed.

To better correlate the drug like properties of the best compounds (**9**, **12–14**, **18**, **20**, **21** and **23**), lipophilicity, expressed as the octanol/water partition coefficient and herein called *log*P, as well as other theoretical calculations such as topological polar surface area (TPSA), number of hydrogen acceptors, number of hydrogen bond donors, volume and rotatable bonds, were calculated using the Molinspiration Cheminformatics software (Table S2) [29]. All the studied compounds comply with Lipinski's rule of five and, therefore, present good characteristics that make them suitable as potential drug candidates.

3. Conclusions

8-Substituted coumarins have been less explored as *h*MAO-A and *h*MAO-B inhibitors than 3, 6 or 7. Therefore, a series of 8-amide and 8-carbamatecoumarins have been design, synthesized, and evaluated on the two *h*MAO isoforms. This exploratory study led to the identification of *N*-(7-hydroxy-4-methylcoumarin-8-yl)-4-methylbenzamide (**9**) as the most active and selective *h*MAO-A inhibitor within the series ($IC_{50} = 15.0$ nM), presenting a good ability to cross the BBB, assessed by the PAMPA assay. This irreversible *h*MAO-A inhibitor is twenty-four times more active *in vitro* than moclobemide, a current therapeutic option for depression and anxiety. Its coumarin nucleus and the *p*-methylphenyl substituent proved to strongly interact with Phe352, Tyr407 and Phe208 residues of the enzyme binding pocket. The hydroxyl group at position 7 proved to establish a stable hydrogen bond with Asn181. Experimentally, compound **9** proved to be chemically stable at different pHs, with a $t_{1/2}$ of 6.84 min and an intrinsic clearance of $195.63 \mu\text{L min}^{-1} \text{mg}^{-1}$ protein. Finally, all the active compounds within the series showed non-significant cytotoxicity on SH-SY5Y cells. All the favorable theoretical and experimental drug-like properties obtained so far may be the inspiration in the search for new drugs for different pathologies in which MAO-A pathways are involved. The chemical structures of compounds **9** and **12** open new doors for further chemical improvement based on exploring different electron donors and/or positions at the aromatic ring of the benzamide. The chemical structure of compound **18** may inspire the inclusion of differently substituted vinyl amides in the scaffold. Finally, the chemical structure of compound **20** may be the inspiration for introducing carbamates that may increase chemical stability and capability to permeate membranes, as well as modulating new inter- and intramolecular interactions with MAO-A. All this new chemical information may help towards the development of more promising MAO-A inhibitors based on the coumarin scaffold.

4. Experimental Section

4.1. Chemistry

4.1.1. General remarks

Starting materials and reagents were obtained from commercial suppliers (Sigma-Aldrich) and were used without further purification. Melting points (Mp) are uncorrected and were determined with a Reichert Kofler thermopan or in capillary tubes in a Büchi 510 apparatus. ^1H NMR (300 MHz) and ^{13}C NMR (75.4 MHz) spectra were recorded with a Bruker AMX spectrometer using CDCl_3 or $\text{DMSO-}d_6$ as solvent. Chemical shifts (δ) are expressed in parts per million (ppm) using TMS as an internal standard. Coupling constants *J* are expressed in Hertz (Hz). Spin multiplicities are given as s (singlet), d (doublet), t (triplet), q (quartet), p (pentet) and m (multiplet). Mass spectrometry was carried out with a Hewlett-Packard 5988A spectrometer. Elemental analyses were performed by a Perkin-Elmer 240B micro-analyzer and are within $\pm 0.4\%$ of calculated values in all cases. The analytical results document $\geq 98\%$ purity for all compounds. Flash chromatography (FC) was performed on silica gel (Merck 60, 230–400 mesh); analytical TLC was performed on precoated silica gel plates (Merck 60 F254). Organic solutions were dried over anhydrous sodium sulfate. Concentration and evaporation of the solvent after reaction or extraction was carried out on a rotary evaporator (Büchi Rotavapor) operating under reduced pressure. All compounds are $>95\%$ pure by HPLC analysis.

4.1.2. Procedure for the preparation of the 8-amine-7-hydroxy-4-methylcoumarin

The commercially available 7-hydroxy-4-methyl-8-nitrocoumarin (1 mmol) was dissolved in ethanol (10 mL). Palladium on carbon (Pd/C, catalytic amount) was added, and the suspension stirred in hydrogen gas (H_2) atmosphere for 5 h. The batch was evaporated and purified by column chromatography (hexane/EtOAc, 9:1) to give the 8-amine-7-hydroxy-4-methylcoumarin in 90% yield.

4.1.3. General procedure for the preparation of the compounds 1–25

The 8-amine-7-hydroxy-4-methylcoumarin (1 mmol) was dissolved in dichloromethane (5 mL). Pyridine (1.1 mmol) was then added, and the mixture was cooled to 0°C . The corresponding acid chloride (1.1 mmol) was added dropwise at this temperature, and the mixture was stirred overnight at room temperature. The batch was evaporated and purified by column chromatography (hexane/EtOAc, 9:1) to give the desired compound [30–33].

4.1.3.1. *N*-(7-Hydroxy-4-methylcoumarin-8-yl)acetamide (**1**). [30]

4.1.3.2. *N*-(7-Hydroxy-4-methylcoumarin-8-yl)propionamide (**2**). ^1H NMR ($\text{DMSO-}d_6$) δ (ppm), *J* (Hz): 1.09 (t, 3H, CH_3 , $J = 7.4$), 2.38 (q, 2H, CH_2 , $J = 7.4$), 2.44 (s, 3H, CH_3), 6.15 (s, 1H, H-3), 6.88 (d, 1H, H-6, $J = 8.8$), 7.51 (d, 1H, H-5, $J = 8.8$), 9.23 (s, 1H, NH), 10.32 (s, 1H, OH). ^{13}C NMR ($\text{DMSO-}d_6$) δ (ppm): 9.9, 18.4, 28.5, 110.4, 112.4, 112.8, 112.9, 124.0, 154.0, 157.0, 160.1, 172.8, 172.9. EI-MS *m/z* (%): 247.1. Ana. Elem. Calc. for $\text{C}_{13}\text{H}_{13}\text{NO}_4$: C, 63.15; H, 5.30; N, 5.67. Found: C, 63.17; H, 5.35; N, 5.62.

4.1.3.3. *N*-(7-hydroxy-4-methylcoumarin-8-yl)isobutyramide (**3**). ^1H NMR ($\text{DMSO-}d_6$) δ (ppm), *J* (Hz): 1.08 (s, 3H, CH_3), 1.11 (s, 3H, CH_3), 2.35 (s, 3H, CH_3), 2.46 (p, 1H, CH, $J = 6.8$), 6.12 (s, 1H, H-3), 6.86 (d, 1H, H-6, $J = 8.8$), 7.48 (d, 1H, H-5, $J = 8.8$), 9.15 (s, 1H, NH), 10.33 (s, 1H, OH). ^{13}C NMR ($\text{DMSO-}d_6$) δ (ppm): 18.3, 19.7, 34.1, 110.3, 112.4, 112.8, 124.0, 150.5, 154.1, 157.1, 160.1, 176.2. EI-MS *m/z* (%): 261.0. Ana. Elem. Calc. for $\text{C}_{14}\text{H}_{15}\text{NO}_4$: C, 64.36; H, 5.79; N, 5.36. Found: C, 64.34; H, 5.76; N, 5.39.

4.1.3.4. *2'-Chloro-N-(7-hydroxy-4-methylcoumarin-8-yl)acetamide (4)*. [31]

4.1.3.5. *N-(7-hydroxy-4-methylcoumarin-8-yl)acrylamide (5)*. [32]

4.1.3.6. *N-(7-Hydroxy-4-methylcoumarin-8-yl)-3',3'-dimethylbutanamide (6)*. ¹H NMR (DMSO-*d*₆) δ (ppm), *J* (Hz): 1.07 (s, 9H, 3xCH₃), 2.19 (s, 2H, CH₂), 2.44 (s, 3H, CH₃), 6.12 (s, 1H, H-3), 6.85 (d, 1H, H-6, *J* = 8.8), 7.48 (d, 1H, H-5, *J* = 8.8), 9.16 (s, 1H, NH), 10.34 (s, 1H, OH). ¹³C NMR (DMSO-*d*₆) δ (ppm): 18.4, 29.9, 30.9, 49.0, 110.3, 112.4, 112.7, 121.1, 123.9, 150.5, 153.9, 156.9, 160.0, 170.6. EI-MS *m/z* (%): 289.0. Ana. Elem. Calc. for C₁₆H₁₉NO₄: C, 66.42; H, 6.62; N, 4.84. Found: C, 66.47; H, 6.61; N, 4.83.

4.1.3.7. *N-(7-Hydroxy-4-methylcoumarin-8-yl)cyclohexanecarboxamide (7)*. ¹H NMR (DMSO-*d*₆) δ (ppm), *J* (Hz): 0.70–0.76 (m, 6H, 3xCH₂), 0.89–0.93 (m, 4H, 2xCH₂), 1.48–1.52 (m, 1H, CH), 1.62 (s, 3H, CH₃), 6.20 (s, 1H, H-3), 6.92 (d, 1H, H-6, *J* = 8.9), 7.17 (d, 1H, H-5, *J* = 8.9), 9.60 (s, 1H, NH), 10.50 (s, 1H, OH). ¹³C NMR (DMSO-*d*₆) δ (ppm): 10.7, 13.9, 19.6, 20.1, 22.9, 34.5, 46.3, 112.1, 112.9, 114.1, 121.0, 121.8, 145.0, 148.9, 152.3, 161.6, 171.8. EI-MS *m/z* (%): 301.3. Ana. Elem. Calc. for C₁₇H₁₉NO₄: C, 67.76; H, 6.36; N, 4.65. Found: C, 67.79; H, 6.33; N, 4.64.

4.1.4. *N-(7-Hydroxy-4-methylcoumarin-8-yl)benzamide (8)*

¹H NMR (DMSO-*d*₆) δ (ppm), *J* (Hz): 2.39 (s, 3H, CH₃), 6.15 (s, 1H, H-3), 6.95 (d, 1H, H-6, *J* = 8.8), 7.49–7.61 (m, 4H, H-5, H-3', H-4', H5'), 8.00–8.03 (d, 2H, H-2', H-6', *J* = 7.3), 9.71 (s, 1H, NH), 10.53 (s, 1H, OH). ¹³C NMR (DMSO-*d*₆) δ (ppm): 18.7, 110.5, 110.6, 112.7, 113.1, 124.7, 128.3, 128.8, 132.1, 134.4, 151.3, 154.4, 157.9, 160.4, 165.9. EI-MS *m/z* (%): 295.1. Ana. Elem. Calc. for C₁₇H₁₃NO₄: C, 69.15; H, 4.44; N, 4.74. Found: C, 69.10; H, 4.47; N, 4.75.

4.1.4.1. *N-(7-hydroxy-4-methylcoumarin-8-yl)-4'-methylbenzamide (9)*. [33]

4.1.4.2. *N-(7-Hydroxy-4-methylcoumarin-8-yl)-4'-nitrobenzamide (10)*. ¹H NMR (DMSO-*d*₆) δ (ppm), *J* (Hz): 2.33 (s, 3H, CH₃), 6.11 (s, 1H, H-3), 6.98 (d, 1H, H-6, *J* = 8.8), 7.60 (d, 1H, H-5, *J* = 8.8), 8.25 (d, 2H, H-2', H-6', *J* = 8.2), 8.40 (d, 2H, H-3', H-5', *J* = 8.2), 10.13 (s, 1H, NH), 10.67 (s, 1H, OH). ¹³C NMR (DMSO-*d*₆) δ (ppm): 18.4, 110.3, 110.4, 112.4, 112.8, 114.0, 123.8, 123.9, 124.8, 129.5, 140.1, 150.9, 156.8, 157.8, 164.7. EI-MS *m/z* (%): 340.0. Ana. Elem. Calc. for C₁₇H₁₂N₂O₆: C, 60.00; H, 3.55; N, 8.23. Found: C, 59.97; H, 3.56; N, 8.26.

4.1.4.3. *4'-Chloro-N-(7-hydroxy-4-methylcoumarin-8-yl)benzamide (11)*. ¹H NMR (DMSO-*d*₆) δ (ppm), *J* (Hz): 2.39 (s, 3H, CH₃), 6.15 (s, 1H, H-3), 6.96 (d, 1H, H-6, *J* = 8.8), 7.69 (d, 1H, H-5, *J* = 8.8), 7.98–8.16 (m, 4H, H-2', H-3', H-5', H-6'), 9.81 (s, 1H, NH), 10.53 (s, 1H, OH). ¹³C NMR (DMSO-*d*₆) δ (ppm): 18.7, 112.7, 113.1, 115.4, 120.0, 124.8, 128.9, 130.2, 132.4, 144.2, 153.2, 154.4, 157.8, 160.4, 165.0. EI-MS *m/z* (%): 329.0. Ana. Elem. Calc. for C₁₇H₁₂ClNO₄: C, 61.92; H, 3.67; N, 4.25. Found: C, 61.96; H, 3.64; N, 4.24.

4.1.4.4. *N-(7-hydroxy-4-methylcoumarin-8-yl)-4'-methoxybenzamide (12)*. ¹H NMR (DMSO-*d*₆) δ (ppm), *J* (Hz): 2.40 (s, 3H, CH₃), 3.83 (s, 3H, OCH₃), 6.16 (s, 1H, H-3), 6.95 (d, 1H, H-6, *J* = 8.8), 7.06 (d, 1H, H-5, *J* = 8.8), 7.57 (d, 2H, H-3', H-5', *J* = 8.9), 7.99 (d, 2H, H-2', H-6', *J* = 8.9), 9.58 (s, 1H, NH), 10.49 (s, 1H, OH). ¹³C NMR (DMSO-*d*₆) δ (ppm): 18.2, 55.4, 110.1, 112.3, 112.6, 112.8, 113.5, 124.1, 126.1, 129.8, 150.9, 154.0, 157.4, 160.0, 161.9, 165.1. EI-MS *m/z* (%): 325.3. Ana. Elem. Calc. for C₁₈H₁₅NO₅: C, 66.46; H, 4.65; N, 4.31. Found: C, 66.44; H, 4.67; N, 4.33.

4.1.4.5. *3',4'-Dichloro-N-(7-hydroxy-4-methylcoumarin-8-yl)benzamide (13)*. ¹H NMR (DMSO-*d*₆) δ (ppm), *J* (Hz): 2.39 (s, 3H, CH₃), 6.16 (s, 1H, H-3), 6.99 (d, 1H, H-6, *J* = 8.7), 7.58 (d, 1H, H-5, *J* = 8.7), 7.83 (d, 1H, H-5', *J* = 8.7), 7.97 (d, 1H, H-6', *J* = 8.7), 8.17 (s, 1H, H-2'), 9.96 (s, 1H, NH), 10.59 (s, 1H, OH). ¹³C NMR (DMSO-*d*₆) δ (ppm): 18.4, 110.3, 112.1, 112.9, 118.3, 121.3, 127.1, 128.3, 130.0, 131.0, 131.5, 134.6, 142.8, 145.5, 154.1, 157.5, 160.0. EI-MS *m/z* (%): 363.0. Ana. Elem. Calc. for C₁₇H₁₁Cl₂NO₄: C, 56.07; H, 3.04; N, 3.85. Found: C, 56.02; H, 3.00; N, 3.88.

4.1.4.6. *N-(7-Hydroxy-4-methylcoumarin-8-yl)-3',4'-dimethoxybenzamide (14)*. ¹H NMR (DMSO-*d*₆) δ (ppm), *J* (Hz): 2.40 (s, 3H, CH₃), 3.32 (s, 6H, 2xOCH₃), 6.57 (s, 1H, H-3), 7.16 (d, 1H, H-6, *J* = 8.7), 7.52 (s, 1H, H-2'), 7.64–7.77 (m, 3H, H-5, H-5', H-6'), 9.81 (s, 1H, NH), 10.55 (s, 1H, OH). ¹³C NMR (DMSO-*d*₆) δ (ppm): 18.8, 56.5, 112.0, 112.7, 115.3, 117.9, 119.3, 119.5, 120.1, 125.3, 129.2, 137.5, 149.2, 153.2, 154.9, 160.9, 163.2. EI-MS *m/z* (%): 355.1. Ana. Elem. Calc. for C₁₉H₁₇NO₆: C, 64.22; H, 4.82; N, 3.94. Found: C, 64.21; H, 4.79; N, 3.96.

4.1.4.7. *N-(7-Hydroxy-4-methylcoumarin-8-yl)-3',4',5'-trimethoxybenzamide (15)*. ¹H NMR (DMSO-*d*₆) δ (ppm), *J* (Hz): 2.40 (s, 3H, CH₃), 3.79 (s, 3H, OCH₃), 3.87 (s, 6H, 2xOCH₃), 6.58 (s, 1H, H-3), 7.37 (s, 2H, H-2', H-6'), 7.66 (d, 1H, H-6, *J* = 8.8), 8.15 (d, 1H, H-5, *J* = 8.8), 9.76 (s, 1H, NH), 10.49 (s, 1H, OH). ¹³C NMR (DMSO-*d*₆) δ (ppm): 21.8, 56.4, 60.1, 107.7, 112.2, 112.8, 114.1, 119.7, 121.2, 129.5, 139.9, 145.3, 149.1, 152.3, 154.1, 160.6, 169.4. EI-MS *m/z* (%): 385.1. Ana. Elem. Calc. for C₂₀H₁₉NO₇: C, 62.33; H, 4.97; N, 3.63. Found: C, 62.31; H, 4.97; N, 3.65.

4.1.4.8. *N-(7-Hydroxy-4-methylcoumarin-8-yl)furan-2'-carboxamide (16)*. [33].

4.1.4.9. *N-(7-Hydroxy-4-methylcoumarin-8-yl)nicotinamide (17)*. ¹H NMR (DMSO-*d*₆) δ (ppm), *J* (Hz): 2.39 (s, 3H, CH₃), 6.16 (s, 1H, H-3), 6.98 (d, 1H, H-6, *J* = 8.7), 7.60 (d, 1H, H-5, *J* = 8.7), 7.87 (t, 1H, H-5', *J* = 8.9), 8.67–8.93 (m, 2H, H-4', H-6'), 9.12 (s, 1H, H-2'), 9.30 (s, 1H, NH), 10.23 (s, 1H, OH). ¹³C NMR (DMSO-*d*₆) δ (ppm): 18.7, 110.7, 112.0, 112.7, 113.2, 125.1, 125.8, 131.3, 140.2, 146.1, 149.0, 151.2, 154.5, 157.7, 160.3, 163.2. EI-MS *m/z* (%): 296.0. Ana. Elem. Calc. for C₁₆H₁₂N₂O₄: C, 64.86; H, 4.08; N, 9.46. Found: C, 64.83; H, 4.07; N, 9.49.

4.1.5. *N-(7-hydroxy-4-methylcoumarin-8-yl)cinnamamide (18)*

¹H NMR (DMSO-*d*₆) δ (ppm), *J* (Hz): 2.39 (s, 3H, CH₃), 6.17 (s, 1H, H-3), 6.91–6.95 (m, 2H, CH, H-6), 7.42–7.52 (m, 3H, H-3', H-4', H-5'), 7.55 (d, 1H, H-5, *J* = 8.8), 7.58–7.62 (m, 3H, CH, H-2', H-6'), 9.63 (s, 1H, NH), 10.53 (s, 1H, OH). ¹³C NMR (DMSO-*d*₆) δ (ppm): 18.7, 110.8, 112.9, 113.2, 117.3, 122.0, 124.4, 128.2, 129.5, 130.2, 135.2, 140.6, 150.6, 154.4, 157.1, 160.3, 164.8. EI-MS *m/z* (%): 321.2. Ana. Elem. Calc. for C₁₇H₁₃NO₅: C, 71.02; H, 4.71; N, 4.36. Found: C, 71.03; H, 4.70; N, 4.38.

4.1.5.1. *Methyl (7-hydroxy-4-methylcoumarin-8-yl)carbamate (19)*. ¹H NMR (DMSO-*d*₆) δ (ppm), *J* (Hz): 2.37 (s, 3H, CH₃), 3.59 (s, 3H, OCH₃), 6.15 (s, 1H, H-3), 6.88 (d, 1H, H-6, *J* = 8.8), 7.52 (d, 1H, H-5, *J* = 8.8), 8.25 (s, 1H, NH), 10.46 (s, 1H, OH). ¹³C NMR (DMSO-*d*₆) δ (ppm): 18.7, 52.2, 110.5, 110.6, 112.7, 112.9, 124.5, 151.4, 154.4, 155.6, 157.9, 160.4. EI-MS *m/z* (%): 249.0. Ana. Elem. Calc. for C₁₂H₁₁NO₅: C, 57.83; H, 4.45; N, 5.62. Found: C, 57.81; H, 4.47; N, 5.63.

4.1.5.2. *Ethyl (7-hydroxy-4-methylcoumarin-8-yl)carbamate (20)*. ¹H NMR (DMSO-*d*₆) δ (ppm), *J* (Hz): 1.18 (t, 3H, CH₃, *J* = 7.0), 2.38 (s, 3H, CH₃), 4.10 (q, 2H, CH₂, *J* = 7.0), 6.16 (s, 1H, H-3), 6.91 (d, 1H, H-6, *J* = 8.8), 7.60 (d, 1H, H-5, *J* = 8.8), 9.14 (s, 1H, NH), 11.07 (s, 1H, OH). ¹³C NMR (DMSO-*d*₆) δ (ppm): 14.4, 18.7, 63.1, 110.6, 112.6, 112.9, 113.7,

119.1, 126.2, 151.6, 154.6, 157.0, 159.8. EI-MS m/z (%): 263.0. Ana. Elem. Calc. for $C_{13}H_{13}NO_5$: C, 59.31; H, 4.98; N, 5.32. Found: C, 59.28; H, 4.99; N, 5.34.

4.1.5.3. Isopropyl (7-hydroxy-4-methylcoumarin-8-yl)carbamate (21). 1H NMR (DMSO- d_6) δ (ppm), J (Hz): 1.07 (s, 6H, 2xCH₃), 2.32 (s, 3H, CH₃), 4.77 (sp, 1H, CH), 6.09 (s, 1H, H-3), 6.75 (d, 1H, H-6, $J = 8.5$), 6.90 (d, 1H, H-5, $J = 8.5$), 9.14 (s, 1H, NH), 11.07 (s, 1H, OH). ^{13}C NMR (DMSO- d_6) δ (ppm): 18.7, 22.5, 68.1, 110.6, 111.6, 113.0, 120.6, 124.3, 135.5, 147.8, 153.3, 154.8, 163.2. EI-MS m/z (%): 277.1. Ana. Elem. Calc. for $C_{14}H_{15}NO_5$: C, 60.64; H, 5.45; N, 5.05. Found: C, 60.66; H, 5.47; N, 5.01.

4.1.5.4. Isobutyl (7-hydroxy-4-methylcoumarin-8-yl)carbamate (22). 1H NMR (DMSO- d_6) δ (ppm), J (Hz): 0.87 (s, 6H, 2xCH₃), 1.84–1.86 (m, 1H, CH), 2.37 (s, 3H, CH₃), 3.79 (d, 2H, CH₂, $J = 6.5$), 6.14 (s, 1H, H-3), 6.90 (d, 1H, H-6, $J = 8.8$), 7.49 (d, 1H, H-5, $J = 8.8$), 8.51 (s, 1H, NH), 10.52 (s, 1H, OH). ^{13}C NMR (DMSO- d_6) δ (ppm): 18.4, 19.0, 27.8, 70.4, 110.3, 112.3, 112.5, 112.6, 124.1, 144.4, 149.9, 154.1, 155.0, 160.1. EI-MS m/z (%): 291. Ana. Elem. Calc. For $C_{15}H_{17}NO_5$: C, 61.85; H, 5.88; N, 4.81. Found: C, 61.88; H, 5.84; N, 4.79.

4.1.5.5. Chloromethyl (7-hydroxy-4-methylcoumarin-8-yl)carbamate (23). 1H NMR (DMSO- d_6) δ (ppm), J (Hz): 2.34 (s, 3H, CH₃), 5.90 (s, 2H, CH₂), 6.13 (s, 1H, H-3), 6.91 (d, 1H, H-6, $J = 8.8$), 7.52 (d, 1H, H-5, $J = 8.8$), 9.23 (s, 1H, NH), 10.36 (s, 1H, OH). ^{13}C NMR (DMSO- d_6) δ (ppm): 18.4, 63.7, 110.4, 112.4, 112.7, 120.0, 124.5, 150.8, 154.0, 157.0, 159.9, 165.4. EI-MS m/z (%): 283.0. Ana. Elem. Calc. for $C_{12}H_{10}ClNO_5$: C, 50.81; H, 3.55; N, 4.94. Found: C, 50.76; H, 3.58; N, 4.93.

4.1.5.6. Phenyl (7-hydroxy-4-methylcoumarin-8-yl)carbamate (24). 1H NMR (DMSO- d_6) δ (ppm), J (Hz): 2.59 (s, 3H, CH₃), 6.30 (s, 1H, H-3), 7.09 (d, 1H, H-6, $J = 8.7$), 7.80–8.00 (m, 4H, H-5, H-2', H-4', H-6'), 8.87–9.00 (m, 2H, H3', H-5'), 9.92 (s, 1H, NH), 10.21 (s, 1H, OH). ^{13}C NMR (DMSO- d_6) δ (ppm): 18.8, 114.1, 118.5, 119.1, 119.6, 128.1, 128.9, 129.3, 130.1, 149.7, 150.0, 153.9, 159.6, 163.9, 166.1. EI-MS m/z (%): 311.2. Ana. Elem. Calc. for $C_{17}H_{13}NO_5$: C, 65.59; H, 4.21; N, 4.50. Found: C, 65.62; H, 4.25; N, 4.46.

4.1.5.7. Benzyl (7-hydroxy-4-methylcoumarin-8-yl)carbamate (25). 1H NMR (DMSO- d_6) δ (ppm), J (Hz): 2.36 (s, 3H, CH₃), 5.08 (s, 2H, CH₂), 6.14 (s, 1H, H-3), 6.90 (d, 1H, H-6, $J = 8.6$), 7.25–7.37 (m, 5H, H-2', H-3', H-4', H-5', H-6'), 7.53 (d, 1H, H-5, $J = 8.6$), 8.70 (s, 1H, NH), 10.55 (s, 1H, OH). ^{13}C NMR (DMSO- d_6) δ (ppm): 18.7, 66.2, 110.6, 112.7, 112.9, 124.5, 128.0, 128.2, 128.8, 137.3, 151.4, 154.3, 155.0, 157.9, 160.4. EI-MS m/z (%): 325.3. Ana. Elem. Calc. for $C_{18}H_{15}NO_5$: C, 66.46; H, 4.65; N, 4.31. Found: C, 66.49; H, 4.61; N, 4.29.

4.2. Pharmacology

4.2.1. Monoamine oxidases inhibition

The activity of hMAO-A and hMAO-B was evaluated by measuring the amount of H₂O₂ formed from *p*-tyramine, using the Amplex Red Test Kit MAO (Molecular Probes) and the MAO isoforms obtained from insect cells (BTI-TN 5B1-4) infected with baculovirus recombinants containing hMAO-A or hMAO-B cDNA inserts (Sigma-Aldrich). Effects of the compounds 1–25 on the enzymatic activity of hMAO isoforms were evaluated by a fluorimetric method. Briefly, 0.1 mL of sodium phosphate buffer (0.05 M, pH 7.4) containing different concentrations of compounds 1–25 or reference inhibitors and adequate amounts of recombinant hMAO-A or hMAO-B required and adjusted to obtain under our experimental conditions the same reaction velocity [165 pmol of *p*-tyramine per min (hMAO-A: 1.1 μ g of protein; specific activity: 150 nmol of *p*-tyramine oxidized to *p*-hydroxyphenylacetaldehyde/min/mg of

protein; hMAO-B: 7.5 μ g of protein; specific activity: 22 nmol of *p*-tyramine transformed/min/mg of protein)] were placed in a dark fluorimeter chamber and incubated for 10 min at 37 °C. The reaction was started by adding (final concentrations) 200 μ M Amplex Red reagent, 1 U/mL horseradish peroxidase and 1 mM *p*-tyramine. The production of hydrogen peroxide (H₂O₂) and, consequently, of resorufin was quantified at 37 °C in a multidetection microplate fluorescence reader (FluoStar Optima, BMG LABTECH) based on the fluorescence generated (excitation, 545 nm, emission, 590 nm) over a 15 min period, in which the fluorescence increased linearly. Control experiments were carried out simultaneously by replacing the tested drugs with appropriate dilutions of the vehicles. In addition, the possible capacity of the above tested drugs to modify the fluorescence generated in the reaction mixture due to non-enzymatic inhibition (e.g., for directly reacting with Amplex Red reagent) was determined by adding these drugs to solutions containing only the Amplex Red reagent in a sodium phosphate buffer. The specific fluorescence emission (used to obtain the final results) was calculated after subtraction of the background activity, which was determined from wells containing all components except the hMAO isoforms, which were replaced by a sodium phosphate buffer solution [34]. MAO inhibitory activity of the test compounds was expressed as IC₅₀, i.e., the concentration of each drug required to reduce 50% the control value activity for MAO isoforms.

4.2.2. Reversibility study

A dilution method was used to evaluate whether compound 9 is a reversible or irreversible hMAO-A inhibitor [35]. A 100X concentration of the enzyme used in the above described experiments was incubated with a concentration of inhibitor equivalent to 10-fold the IC₅₀ value. After 30 min, the mixture was diluted 100-fold into a reaction buffer containing Amplex Red reagent, horseradish peroxidase and *p*-tyramine and the reaction was monitored for 15 min. Reversible inhibitors show linear progress with a slope equal to $\approx 91\%$ of the slope of the control, whereas irreversible inhibition reaches only $\approx 9\%$ of this slope. A control test was carried out by pre-incubating and diluting the enzyme in the absence of inhibitor.

4.2.3. Cytotoxicity assays

The SH-SY5Y cells grew in a culture medium containing Nutrient Mixture F-12 Ham (Ham's F12) and Minimum Essential Medium Eagle (EMEM) (mixture 1:1) and supplemented with 15% Fetal Bovine Serum (FBS), 1% L-Glutamine, 1% non-essential amino acids (all of them from Sigma-Aldrich S.A.) and 1% of penicillin G/streptomycin sulfate (Gibco, Invitrogen). The cells grew in 75 cm² flask in an incubator, under conditions of saturated humidity with a partial pressure of 5% CO₂ in the air, at 37 °C, until reaching the confluence, 90–95% of the flask surface. To carry out the cytotoxicity assays, the cells were seeded in sterile 96-well plates, with a density of 2×10^5 cells/mL and grown distributed in aliquots of 100 μ L for 24 h under the conditions above described.

Subsequently, the cultures were treated with the compounds dissolved in DMSO, at 100 μ M concentration (1% DMSO) and incubated for 24 h. After this time, cell viability was determined using 3-bromide-(4,5-dimethyl-2-thiazoyl)-2,5-diphenyltetrazolium (MTT). 10 μ L of MTT solution (5 mg/mL in Hank's) were added to each well containing 100 μ L of culture medium and the cells were incubated for 2 h as above described. Then, culture medium was removed, 100 μ L DMSO/well was added to solve the formazan crystals formed by the viable cells and the absorbance (λ 540 nm) was quantified in a plate reader. The viability (percentage) was calculated as [Absorbance (treatment)/Absorbance (negative control)]100% [36].

4.2.4. In vitro metabolic stability using human and mouse liver microsomes

Human and mouse microsomes from Xenotech were employed in the assay. They content 20 mg/mL of protein. The following quantities were

added to each well of a 96-well microplate.

Phosphate buffer Na/K 50 mM pH 7.4		Human (μL)	Mouse (μL)
		299	310
MgCl₂ 30 mM	COFACTORS	163	163
NADP 10 mM			
Glucose 6-P 100 mM			
Glucose 6-P DH 40 U/mL			
Human microsomes		33.1	–
Mouse microsomes		–	22.4
Test compound		5	5
Total volume (μL)		500	500

Plates were incubated at 37 °C and 75 μL samples were taken at 0, 10, 20, 40 and 60 min. Samples were transferred to a microplate and 75 μL Acetonitrile + IS(Rolipram) were added for inactivating the microsomes, and 30 μL of H₂O with 0.5% formic acid for improving the chromatographic conditions and kept at 4 °C. When all the samples were taken the plate was centrifuged at 46000 g for 30 min at 15 °C.

The assay was carried out in a robotic liquid handling system (Caliper). All incubations were performed individually for each test compound. Compounds (1 μM) were incubated in 96-well plates at 37 °C during 1 h under standard incubation conditions: sodium-potassium phosphate buffer (50 mM, pH 7.4), MgCl₂ (3 mM), the NADPH-regenerating system and human or mouse microsomes; CYP content (0.3 nmol/mL). At preset times (0, 10, 20, 40 and 60 min) aliquots of the reaction mixture were stopped with an equal volume of cold acetonitrile. Upon centrifugation of the resultant mixture, supernatants were analysed by a generic UPLC-MS/MS method. The assay was performed with an UPLC QSM Waters Acquity using the following chromatographic conditions.

1. Flow: 0.6 mL/min.
2. Stationary phase: Acquity UPLC® BEHC18 1,7 μm (2.1 mm \times 50 mm) (Waters).
3. Mobile phase: A: 0.1% formic; B: acetonitrile+0.1% formic acid. Gradient:

Time (min)	A	B
0	95%	5%
0.1	95%	5%
1	0%	100%
2.5	0%	100%
2.6	95%	5%
3	95%	5%

Metabolic stability was determined by the disappearance of compound over time. Ln-linear plots of the % of compound remaining based on chromatographic peak area *versus* time were plotted, and the slope was calculated by linear fitting of the curve. The *in vitro* metabolic half-life ($t_{1/2}$) was estimated by using the equation $0.693/k$ where k is the biotransformation rate constant and corresponds to the slope of the Ln-linear curve. The microsomal intrinsic clearance (Clint) was calculated using the equation: $\text{Clint} = [V \cdot 0.693] / t_{1/2}$ where V ($\mu\text{L}/\text{mg}$) corresponds to incubation volume (μL)/protein in the incubation (mg). The chart obtained is included in the [Supporting Information](#).

4.2.5. Chemical stability at pH 3.0, 7.4 and 10.0

In order to evaluate chemical stability of compound **9**, overnight incubations of 10 μM , at room temperature, and different pH, were carried out. The follow working solutions have been freshly prepared and used.

1. pH 3.5: CH₃COONa/CH₃COOH 0.1 M
2. pH 7.4: NaH₂PO₄/NaHPO₄ 10 mM

3. pH 10.4: NaHCO₃/Na₂CO₃ 0.5 M

Aliquots at $t = 0$ and after overnight incubation were taken and analysed by UPLC-MSMS. The chromatograms obtained are included in the [Supporting Information](#).

4.2.6. *In vitro* blood–brain barrier permeation assay (PAMPA-BBB)

Prediction of the brain penetration was evaluated using a parallel artificial membrane permeation assay (PAMPA-BBB), in a similar manner as previously described [25–28]. Pipetting was performed with a semi-automatic pipettor (CyBi®-SELMA) and UV reading with a microplate spectrophotometer (Multiskan Spectrum, Thermo Electron Co.). Commercial drugs, phosphate buffered saline solution at pH 7.4 (PBS), dodecane, PVDF membrane filters (diameter 25 mm, pore size 0.45 μm) were purchased from Merck. The porcine brain lipid (PBL) was obtained from Avanti Polar Lipids. The donor microplate was a 96-well filter plate (PVDF membrane, pore size 0.45 μm) and the acceptor microplate was an indented 96-well plate, both from Millipore. The acceptor 96-well microplate was filled with 200 μL of PBS:ethanol (70:30) and the filter surface of the donor microplate was impregnated with 5 μL of porcine brain lipid (PBL) in dodecane (20 mg mL⁻¹). Compounds were dissolved in PBS:ethanol (70:30) at 100 μg mL⁻¹, filtered through a Millex filter, and then added to the donor wells (200 μL). The donor filter plate was carefully put on the acceptor plate to form a sandwich, which was left undisturbed for 120 min at 25 °C. After incubation, the donor plate is carefully removed and the concentration of compounds in the acceptor wells was determined by UV-Vis spectroscopy. Every sample is analysed in four wells in three independent runs, and the results are given as the mean \pm standard deviation. In each experiment, 10 quality control standards of known BBB permeability were included to validate and normalize the analysis set.

4.3. Molecular modelling of compounds **9** and **20** hMAOs interaction

The hMAOs molecular recognition of the most potent and hMAO-A selective **9** and **20** was investigated by means of molecular modelling techniques. The Protein Data Bank (PDB) [37] crystallographic structures 2Z5X [38] and 6FW0 [39] were considered as hMAO-A and hMAO-B computational models, respectively. The original PDB structures were suitable optimized by means of Protein Preparation Wizard tool [40] before the docking studies. Hydrogen atoms were added, the co-crystallized water molecules and inhibitors removed, and the FAD connectivity fixed. OPLS-2005 force field [41] was used to energy minimize the target models.

Glide docking software [42] was used for ligands-targets recognition analyses. The binding site of both hMAO-A and -B theoretical models was mimicked by a regular 64,000 Å^3 box centered on the FAD N5. The standard precision (SP) Glide ligand flexible algorithm was applied to all docking simulation. The Glide GScore scoring function was used for raking the stability of theoretical complexes.

Molecular Dynamics (MD) simulations were carried out on the best docking poses of compounds **9** and **20** by using the Desmond program [43,44]. The system was solvated by means of the SPC explicit solvation model in an orthorhombic shape box [45,46]. The net charge of the resulting system was neutralized by randomly placing 2 Cl⁻ and 3 Na⁺ counterions to the hMAO-A and hMAO-B models, respectively. MD protocol consisted of preliminary system relaxation steps, carried out with Desmond default parameters, followed by the production runs performed in the isothermal isobaric ensemble model (NPT) at 300 °K with a pressure equal to 1 bar. The production MD runs were carried out up to 50 ns, with an integration time step equal to 2 fs. The structure MD trajectories and the energy contributions have been sampled at regular intervals of 50 ps. SHAKE algorithm has been applied to all hydrogen atoms to prevent unrealistic distortion of atoms position [47,48]. The ligand-target interaction analysis was carried out by namesake Desmond tool.

4.4. Theoretical properties

For the theoretical prediction of the physical-chemical properties (i.e. the passage of molecules through biological membranes), Molinspiration Cheminformatics software has been used [29].

Declaration of competing interest

The authors declare that they have no known competing financial interests or personal relationships that could have appeared to influence the work reported in this paper.

Data availability

Data will be made available on request.

Acknowledgements

This research was funded by Consellería de Cultura, Educación e Ordenación Universitaria (EM2014/016), Ministerio de Ciencia e Innovación (PID2020-116076RJ-I00/AEI/10.13039/501100011033) and Fundação para a Ciência e Tecnologia (PTDC/ASP-PES/28397/2017, CEECIND/02423/2018, UIDB/00081/2020, LA/P/0056/2020 and EXPL/BIA-BQM/0492/2021). Financial support from the Xunta de Galicia (Centro de investigación de Galicia accreditation 2019–2022) and the European Union (European Regional Development Fund - ERDF), is also gratefully acknowledged. M.I.R.-F. acknowledges the economic support from the Spanish Ministry of Science, Innovation and Universities; Spanish Research Agency; and European Regional Development Funds (grant PID2021-1226500B-I00) and from CSIC (PIE-202080E118).

Appendix A. Supplementary data

Supplementary data to this article can be found online at <https://doi.org/10.1016/j.ejmech.2023.115091>.

References

- R. Hong, X. Li, Discovery of monoamine oxidase inhibitors by medicinal chemistry approaches, *MedChemComm* 10 (1) (2018) 10–25.
- M.B.H. Youdim, D. Edmondson, K.F. Tipton, The therapeutic potential of monoamine oxidase inhibitors, *Nat. Rev. Neurosci.* 7 (2006) 295–309.
- G. Ferino, S. Vilar, M.J. Matos, E. Uriarte, E. Cadoni, Monoamine oxidase inhibitors: ten years of docking studies, *Curr. Top. Med. Chem.* 12 (2012) 2145–2162.
- J.P. Finberg, J.M. Rabey, Inhibitors of MAO-A and MAO-B in psychiatry and neurology, *Front. Pharmacol.* 7 (2016) 340.
- E. Molina, E. Sobarzo-Sánchez, A. Speck-Planche, M.J. Matos, E. Uriarte, L. Santana, M. Yáñez, F. Orallo, Monoamine oxidase A: an interesting pharmacological target for the development of multi-target QSAR models, *Mini Rev. Med. Chem.* 12 (2012) 947–958.
- M.J. Matos, D. Viña, S. Vázquez-Rodríguez, E. Uriarte, L. Santana, Focusing on new monoamine oxidase inhibitors: differently substituted coumarins as an interesting scaffold, *Curr. Top. Med. Chem.* 12 (2012) 2210–2239.
- G. Delogu, M.J. Matos, Coumarins as promising scaffold for the treatment of age-related diseases – an overview of the last five years, *Curr. Top. Med. Chem.* 17 (29) (2017) 3173–3189.
- M.J. Matos, D. Viña, E. Quezada, C. Picciau, G. Delogu, F. Orallo, L. Santana, E. Uriarte, A new series of 3-phenylcoumarins as potent and selective MAO-B inhibitors, *Bioorg. Med. Chem. Lett.* 19 (2009) 3268–3270.
- M.J. Matos, D. Viña, C. Picciau, F. Orallo, L. Santana, E. Uriarte, Synthesis and evaluation of 6-methyl-3-phenylcoumarins as potent and selective MAO-B inhibitors, *Bioorg. Med. Chem. Lett.* 19 (2009) 5053–5055.
- M.J. Matos, D. Viña, P. Janeiro, F. Borges, L. Santana, E. Uriarte, New halogenated 3-phenylcoumarins as potent and selective MAO-B inhibitors, *Bioorg. Med. Chem. Lett.* 20 (2010) 5157–5160.
- M.J. Matos, C. Terán, Y. Pérez-Castillo, E. Uriarte, L. Santana, D. Viña, Synthesis and study of a series of 3-arylcoumarins as potent and selective monoamine oxidase B inhibitors, *J. Med. Chem.* 54 (2011) 7127–7137.
- D. Viña, M.J. Matos, G. Ferino, E. Cadoni, R. Laguna, F. Borges, E. Uriarte, L. Santana, 8-Substituted-3-arylcoumarins as potent and selective MAO-B inhibitors: synthesis, pharmacological evaluation and docking studies, *ChemMedChem* 7 (2012) 464–470.
- M.J. Matos, S. Vázquez-Rodríguez, E. Uriarte, L. Santana, D. Viña, MAO inhibitory activity modulation: 3-phenylcoumarins versus 3-benzoylcoumarins, *Bioorg. Med. Chem. Lett.* 21 (2011) 4224–4227.
- A. Fonseca, M.J. Matos, J. Reis, Y. Duarte, M. Gutiérrez, L. Santana, E. Uriarte, F. Borges, Exploring coumarin potentialities: development of new MAO-B inhibitors based on the 6-methyl-3-carboxamidocoumarin scaffold, *RSC Adv.* 6 (2016) 49764–49768.
- A. Fonseca, J. Reis, T. Silva, M.J. Matos, D. Bagetta, F. Ortuso, S. Alcaro, E. Uriarte, F. Borges, Coumarin versus chromone monoamine oxidase B inhibitors: Quo vadis? *J. Med. Chem.* 60 (16) (2017) 7206–7212.
- D. Viña, M.J. Matos, M. Yáñez, L. Santana, E. Uriarte, 3-Substituted coumarins as dual inhibitors of AChE and MAO for the treatment of Alzheimer's disease, *MedChemComm* 3 (2012) 213–218.
- M.J. Matos, S. Vilar, R.M. Gonzalez-Franco, E. Uriarte, L. Santana, C. Friedman, N. P. Tatonetti, D. Viña, J.A. Fontenla, Novel (coumarin-3-yl)carbamates as selective MAO-B inhibitors: synthesis, in vitro and in vivo assays, theoretical evaluation of ADME properties and docking study, *Eur. J. Med. Chem.* 63 (2013) 151–161.
- M.J. Matos, F. Rodríguez-Enríquez, F. Borges, L. Santana, E. Uriarte, M. Estrada, M. I. Rodríguez-Franco, R. Laguna, D. Viña, 3-Amidocoumarins as potential multifunctional agents against neurodegenerative diseases, *ChemMedChem* 10 (2015) 2071–2079.
- M. Yang, C.-H. Luo, Y.-Q. Zhu, Y.-C. Liu, Y.-J. An, J. Iqbal, Z.-Z. Wang, X.-M. Ma, 7,8-Dihydroxy-4-methylcoumarin reverses depression model-induced depression-like behaviors and alteration of dendritic spines in the mood circuits, *Psychoneuroendocrinology* 119 (2020), 104767.
- S.C. Baek, M.G. Kang, J.E. Park, J.P. Lee, H. Lee, H.W. Ryu, C.M. Park, D. Park, M. L. Cho, S.R. Oh, H. Kim, Osthenol, a prenylated coumarin, as a monoamine oxidase A inhibitor with high selectivity, *Bioorg. Med. Chem. Lett.* 29 (2019) 839–843.
- J.S. Robinson, J.P. Petzer, A. Petzer, J.J. Bergh, A.C. Lourens, Selected furochalcones as inhibitors of monoamine oxidase, *Bioorg. Med. Chem. Lett.* 23 (2013) 4985–4989.
- A.E. Nardi, Antidepressants in social anxiety disorder, *Arq. Neuropsiquiatr.* 59 (3-A) (2001) 637–642.
- C. Zhuo, X. Zhu, R. Jiang, F. Ji, Z. Su, R. Xue, Y. Zhou, Comparison for efficacy and tolerability among ten drugs for treatment of Parkinson's disease: a network meta-analysis, *Sci. Rep.* 8 (2017) 458–465.
- L. Di, E.H. Kerns, K. Fan, O.J. McConnell, G.T. Carter, High throughput artificial membrane permeability assay for blood–brain barrier, *Eur. J. Med. Chem.* 38 (2003) 223–232.
- C. Herrera-Arozamena, M. Estrada-Valencia, P. López-Caballero, C. Pérez, J. A. Morales-García, A. Pérez-Castillo, E. del Sastre, C. Fernández-Mendivil, P. Duarte, P. Michalska, J. Lombardía, S. Senar, R. León, M.G. López, M. I. Rodríguez-Franco, Resveratrol-based MTDLs to stimulate defensive and regenerative pathways and block early events in neurodegenerative cascades, *J. Med. Chem.* 65 (6) (2022) 4727–4751.
- C. Herrera-Arozamena, M. Estrada-Valencia, C. Pérez, L. Lagartera, J.A. Morales-García, A. Pérez-Castillo, J.F. Franco-Gonzalez, P. Michalska, P. Duarte, R. León, M. G. López, A. Mills, F. Gago, Á.J. García-Yagüe, R. Fernández-Ginés, A. Cuadrado, M.I. Rodríguez-Franco, Tuning melatonin receptor subtype selectivity in oxadiazolone-based analogues: discovery of QR2 ligands and NRF2 activators with neurogenic properties, *Eur. J. Med. Chem.* 190 (2020), 112090.
- C. Herrera-Arozamena, M. Estrada-Valencia, O. Martí-Marí, C. Pérez, M. de la Fuente Revenga, C.A. Villalba-Galea, M.I. Rodríguez-Franco, Optical control of muscular nicotinic channels with Azocurioniums, photoswitchable azobenzenes bearing two N-methyl-N-Carbocyclic quaternary ammonium groups, *Eur. J. Med. Chem.* 200 (2020), 112403.
- M. Estrada Valencia, C. Herrera-Arozamena, L. de Andrés, C. Pérez, J.A. Morales-García, A. Pérez-Castillo, E. Ramos, A. Romero, D. Viña, M. Yáñez, E. Laurini, S. Pricl, M.I. Rodríguez-Franco, Neurogenic and neuroprotective Donepezil-Flavonoid hybrids with Sigma-1 affinity and inhibition of key enzymes in Alzheimer's disease, *Eur. J. Med. Chem.* 156 (2018) 534–553.
- Molinspiration Cheminformatics software. <https://www.molinspiration.com>.
- M.A. Pathak, J.H. Fellman, K.D. Kaufman, The effect of structural alterations on the erythral activity of furocoumarins: psoralens, *J. Invest. Dermatol.* 35 (1960) 165–183.
- J.R. Merchant, P.M. Pathare, N.M. Shinde, Synthesis of pyranobenzoxazoles and 2-chloromethylpyranobenzoxazoles, *Curr. Sci.* 53 (8) (1984) 424–425.
- K.M. Amin, Synthesis of oxazinones and acryloyl derivatives of o-aminohydroxycoumarins. *Egypt. J. Pharma. Sci.* 27 (1–4) (1986) 333–340.
- S. Hao, K. Miao, Y. Wei, T. Wang, Preparation of amido hydroxymethyl coumarin compound as acaricide, *Faming Zhuanli Shenqing* (2017), CN107011306. A20170804.
- M. Yáñez, N. Fraiz, E. Cano, F. Orallo, Inhibitory effects of cis- and trans-resveratrol on noradrenaline and 5-hydroxytryptamine uptake and on monoamine oxidase activity, *Biochem. Biophys. Res. Commun.* 344 (2006) 688–695.
- R.A. Copeland, *Evaluation of Enzyme Inhibitors in Drug Discovery*, Wiley Interscience, Hoboken, 2005.
- Y. Liu, D.A. Peterson, H. Kimura, D.J. Schubert, Mechanism of cellular 3-(4,5-dimethylthiazol-2-yl)-2,5-diphenyltetrazolium bromide (MTT) reduction, *Neurochem* 69 (1997) 581–593.
- H.M. Berman, J. Westbrook, Z. Feng, G. Gilliland, T.N. Bhat, H. Weissig, I. N. Shindyalov, P.E. Bourne, The protein Data Bank, *Nucleic Acids Res.* 28 (2000) 235–242.
- S.-Y. Son, J. Ma, Y. Kondou, M. Yoshimura, E. Yamashita, T. Tsukihara, Structure of human monoamine oxidase A at 2.2-Å resolution: the control of opening the entry for substrates/inhibitors, *Proc. Natl. Acad. Sci. USA* 105 (2008) 5739–5744.

- [39] J. Reis, N. Manzella, F. Cagide, J. Mialet-Perez, E. Uriarte, A. Parini, F. Borges, C. Binda, Tight-binding inhibition of human monoamine oxidase B by chromone analogs: a kinetic, crystallographic, and biological analysis, *J. Med. Chem.* 61 (2018) 4203–4212.
- [40] Schrödinger Release 2021-4: Protein Preparation Wizard, Schrödinger, LLC, New York, NY, USA, 2021.
- [41] J.L. Banks, H.S. Beard, Y. Cao, A.E. Cho, W. Damm, R. Farid, A.K. Felts, T. A. Halgren, D.T. Mainz, J.R. Maple, Integrated modeling program, applied chemical theory (IMPACT), *J. Comput. Chem.* 26 (2005) 1752–1780.
- [42] Schrödinger Release 2021-4: Glide, Schrödinger, LLC, New York, NY, USA, 2021.
- [43] Schrödinger Release 2021-4: Desmond Molecular Dynamics System, D. E. Shaw Research; Maestro-Desmond Interoperability Tools, Schrödinger, New York, NY, USA, 2021.
- [44] K.J. Bowers, D.E. Chow, H. Xu, R.O. Dror, M.P. Eastwood, B.A. Gregersen, J. L. Klepeis, I. Kolossvary, M.A. Moraes, F.D. Sacerdoti, Scalable algorithms for molecular dynamics simulations on commodity clusters, in: *Proceedings of the SC'06: 2006 ACM/IEEE Conference on Supercomputing*, Tampa, FL, USA, 11–17 November, 2006, p. 43.
- [45] H.J. Berendsen, J.P. Postma, W.F. van Gunsteren, J. Hermans, Interaction models for water in relation to protein hydration, in: *Intermolecular Forces*, Springer, Dordrecht, The Netherlands, 1981, pp. 331–342.
- [46] M. Fuhrmans, B.P. Sanders, S.-J. Marrink, A.H. de Vries, Effects of bundling on the properties of the SPC water model, *Theor. Chem. Acc.* 125 (2010) 335–344.
- [47] J.-P. Ryckaert, G. Ciccotti, H.J. Berendsen, Numerical integration of the cartesian equations of motion of a system with constraints: molecular dynamics of n-alkanes, *J. Comput. Phys.* 23 (1977) 327–341.
- [48] E. Barth, K. Kuczera, B. Leimkuhler, R.D. Skeel, Algorithms for constrained molecular dynamics, *J. Comput. Chem.* 16 (1995) 1192–1209.